Optica Applicata, Vol. XLVI, No. 2, 2016
DOI: 10.5277/oa160205

Numerical model of a semiconductor disk laser

ADAM K. SOKÓŁ*, ROBERT P. SARZAŁA

Institute of Physics, Lodz University of Technology, ul. Wólczańska 219, 90-924 Łódź, Poland

*Corresponding author: adam.sokol@p.lodz.pl

In this paper we describe the numerical model of a semiconductor disk laser, developed and implemented in the Photonics Group, Institute of Physics, Lodz University of Technology, Poland. It consists of four strongly interrelated components for: carrier transport, heat flow, material gain and optical phenomena calculations. Combination of these components gives the steady-state self-consistent model which enables a simulation of various aspects of a semiconductor disk laser operation. A numerical analysis of carrier and power losses within the active region of 1.3-μm GaInNAs/GaAs semiconductor disk laser has been carried out using this model.

Keywords: semiconductor disk laser (SDL), vertical-external-cavity surface-emitting laser (VECSEL), computer simulation, numerical modelling.

1. Introduction

Semiconductor disk lasers (SDLs), also known as vertical-external-cavity surface-emitting lasers (VECSELs), combine advantages of vertical-cavity surface-emitting lasers (VCSELs), edge-emitting lasers (EELs) and solid-state disk lasers [1]. They can emit relatively high-power radiation with diffraction-limited circularly-symmetric beams. Moreover, their external cavities enable placing additional optical elements within a laser resonator for advanced transverse-mode control, frequency doubling, high repetition rate short pulse generation and so on. Unique properties of SDLs cause that they find many scientific and commercial applications for example in: telecommunication, colour projection displays, broadly defined bioinstrumentation, gas sensing, fingerprint and trace evidence detection or laser shows.

Figure 1 shows a typical SDL structure in a linear optical cavity. A semiconductor chip consisting of a quantum well (QW) active region and a distributed Bragg reflector (DBR), is attached to a heat sink cooled by water or by a Peltier module. The active region is closed by a carrier-confinement window and alternatively by a protective cap layer, which prevents bottom layers for example from oxidation. Sometimes there is also a high-thermal-conductivity heat spreader bonded to the laser upper surface which improves thermal properties of the device. The SDL structure acts as the active mirror

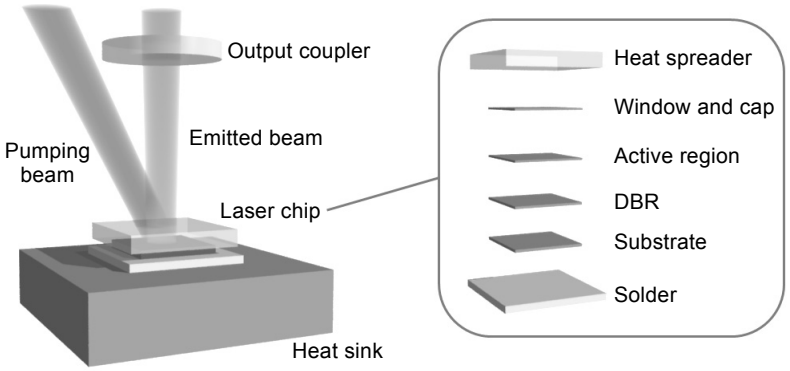

Fig. 1. Typical SDL structure in a linear external cavity.

in an external cavity. In the presented case, the cavity extends from the DBR to the output coupler. The active region is pumped by laser radiation of properly chosen wavelength generated for example by diode lasers or their arrays.

Designing of efficient SDL structures requires deep understanding not only of physical phenomena taking place within their volumes but also of complex interrelations between individual processes, which are often difficult or even impossible to analyse with traditional experimental methods. Numerical analysis brings a solution to this problem. This approach is not only efficient considering time and cost of initial calculations, but is also useful in an optimization process when a number of parameters has to be investigated. In this paper we present the numerical model of a semiconductor disk laser developed and implemented in the Photonics Group, Institute of Physics, Lodz University of Technology, Poland. It consists of four main components for: carrier transport, heat flow, material gain and optical phenomena calculations. These components may be used as separated blocks to analyse individual physical processes or they may be combined in the self-consistent model. Such a model enables an accurate analysis of interrelations between individual physical phenomena taking place within laser volumes so it may be used in complex analysis of SDL operation. There are some numerical models developed by other groups for carrier transport [2–4], thermal [5] and output power [2, 4] calculations in SDLs. However, their descriptions are sometimes not detailed enough or they suffer from various limitations, as discussed in the next sections. The model presented in this paper contains some novel approaches, which enable more accurate analysis of SDL.

In the successive sections we describe the individual model components for: carrier transport, heat flow and optical phenomena calculations as well as the algorithm of the self-consistent model. The gain model has been described in our previous paper [6]. In all our considerations we use the cylindrical (r, z) coordinate system assuming a cylindrical symmetry of a laser structure and a pumping beam. Then we present results of a numerical analysis of carrier and power losses carried out using the described model for 1.3-μm GaInNAs/GaAs semiconductor disk laser.

2. Carrier transport

Active region of a typical SDL structure consists of a number of QWs separated by barrier layers which absorb pumping radiation. Charge carriers generated in these layers diffuse throughout the volume of the whole active region, thermalise and recombine in the spontaneous or stimulated way both in the barriers and QWs. In this scenario, the simulation of carrier transport requires solving a complex 2D diffusion equations (assuming the cylindrical symmetry of the structure and pumping beam) for each barrier layer. Since this approach is difficult and time-consuming, the problem is usually reduced to the 1D carrier transport. In the model from paper [2] only the radial diffusion is considered. Conversely, in the model from [3, 4] the radial direction is not taken into account and only the vertical transport in a laser axis is simulated. However, in both cases there is no information how ignoring one of the directions influences the modelling accuracy. Our model described in this section tries to reconcile these two approaches. Results described in the next section show that the radial carrier transport may be neglected under certain conditions and 2D carrier distributions in an active region may be determined solving a number of independent vertical diffusion equations for successive values of r.

2.1. Radial transport

To determine a radial distribution of carrier density in a single QW, we solve the following radial diffusion equation:

$$D_A\left[\frac{\mathrm{d}^2 n(r)}{\mathrm{d}r^2} + \frac{1}{r}\frac{\mathrm{d}n(r)}{\mathrm{d}r}\right] - \left[An(r) + Bn^2(r) + Cn^3(r)\right] + G(r) = 0 \qquad (1)$$

where D_A is ambipolar diffusion coefficient, n is carrier density, A, B, C are monomolecular, bimolecular and Auger recombination coefficients, respectively, and G is the carrier generation rate whose radial distribution depends directly on the pumping beam intensity profile.

Exemplary results of calculations carried out for the GaInNAs/GaAs quantum well, assuming Gaussian or top-hat profile of the generation rate G, are presented in Fig. 2. Values of ambipolar diffusion coefficient D_A from 0 to 10000 cm^{-1} have been considered. One can see that carrier distributions calculated for $D_A = 0$ and $D_A = 100$ cm^{-1} are very similar. The only exception is the noticeable difference near the sharp edge of the top-hat profile. However, in real top-hat pumping beams this edge is more or less smooth and the intensity profile of such beams is described rather by the super -Gaussian function than the ideal top-hat one. In that case, the difference between carrier distributions for $D_A = 0$ and $D_A = 100$ cm^{-1} is not so evident. Typical semiconductor material systems as: arsenides, phosphides or nitrides have ambipolar diffusion coefficient from 0 to 100 cm^{-1} range. Results presented in Fig. 2 show that for such values of D_A, diffusion has a very limited influence on the radial carrier distribution.

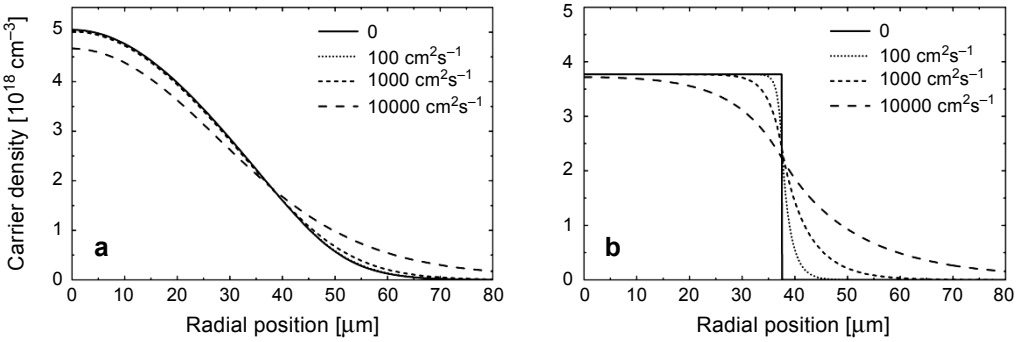

Fig. 2. Radial distributions of carrier density in the GaInNAs/GaAs QW for different values of ambipolar diffusion coefficient for the carrier generation rate described by the Gaussian (**a**) and top-hat (**b**) profiles.

In fact, it is determined mostly by the profile of the carrier generation rate and values of recombination coefficients. Therefore, we can ignore the radial carrier transport in our calculations and focus only on the vertical one.

2.2. Vertical transport

To calculate the carrier density distribution along the active region consisting of N QWs surrounded by $(N + 1)$ barriers, we solve the following one-dimensional diffusion equation with no carrier drift contribution for each barrier [3]:

$$D_A \frac{\mathrm{d}^2 n_b(z)}{\mathrm{d}z^2} - \frac{n_b(z)}{\tau(z)} + G(z) = 0 \tag{2}$$

where D_A is ambipolar diffusion coefficient, n_b is carrier density in barrier, G is carrier generation rate per unit volume and τ is carrier lifetime:

$$\frac{1}{\tau(z)} = A + Bn_b(z) + Cn_b^2(z) \tag{3}$$

where A, B, C are recombination coefficients. Analytical solution of Eq. (2) for the individual barrier is:

$$n_b(z) = C_1 \exp\left(\frac{z}{\sqrt{D_A \tau}}\right) + C_2 \exp\left(-\frac{z}{\sqrt{D_A \tau}}\right) + \frac{q_p \alpha_p \tau}{(1 - \alpha_p^2 D_A \tau)\hbar \omega_p} \exp(-\alpha_p z) \tag{4}$$

where C_1, C_2 are constants, q_p is surface power density of pumping radiation entering the laser active region, α_p is absorption coefficient for pumping radiation, $\hbar$ is the Dirac constant and ω_p is pumping angular frequency. Solutions of Eq. (2) for the individual barriers are connected assuming that there is no carrier flow outside the active region and the carrier density is continuous at each QW. In our model, the QWs are

reduced to points and act as carrier absorbers. Carrier losses in the individual QW can be calculated using the steady-state carrier balance equation:

$$J_L - J_P = d_{\mathrm{QW}}\left(An_{\mathrm{QW}} + Bn_{\mathrm{QW}}^2 + Cn_{\mathrm{QW}}^3 + \sum_m L_{\mathrm{st}}^{(m)}\right) \tag{5}$$

where J_L and J_P are carrier flux densities into the continuous states above the QW from the left and right barrier, respectively, d_{QW} is the QW thickness and n_{QW} is the carrier density in the QW, which is determined by finding the quasi-Fermi levels and calculating the density integrals, $L_{\mathrm{st}}^{(m)}$ is the hole burning rate due to stimulated emission for the m-th transverse mode expressed as:

$$L_{\mathrm{st}}^{(m)}(P^{(m)}, r) = P^{(m)} \frac{f_e^{(m)}(r)}{2\pi\int f_e^{(m)}(r) r \mathrm{d}r} \frac{n_R^{(m)}(r) g^{(m)}(r)}{\hbar\omega_e^{(m)}(r)} \frac{I_{\mathrm{QW}}^{(m)}(r)}{I_{\mathrm{air}}^{(m)}(r)} \tag{6}$$

where P is output power, f_e is a normalised intensity profile for the given mode, n_R is refractive index of the QW material, g is the material gain of the QW, $\hbar$ is the Dirac constant and ω_e is emission angular frequency, I_{QW} and I_{air} are light intensities in the QW and in the air outside the laser cavity, respectively.

The above equations enable determining the vertical carrier distribution in the active region for a given distance from the laser axis. The following algorithm is used. First, an initial carrier density in the first QW (looking from the laser upper surface) is assumed. Using Eqs. (4)–(6) and condition of continuity, carrier density in the subsequent QWs is calculated. Then the derivative of carrier density at the bottom boundary of the active region is determined. Assuming that there is no carrier flow outside the active region, this derivative should be equal to zero. The carrier density in the first QW is being changed until this condition is met. Then, assuming the cylindrical symmetry of the pumping and emitted beams and ignoring the radial carrier transport (as discussed in Section 2.1), we obtain the 3D carrier distribution just by calculating a number of vertical distributions for successive values of r.

3. Heat flow

Knowledge of a temperature distribution within the laser structure is very important as the majority of parameters used in carrier transport, gain and optical model parts are temperature-dependent. Such a distribution may be obtained by solving the 3D Fourier–Kirchhoff heat transfer equation in the cylindrical (r, z) coordinate system [7]:

$$-\mathrm{div}[\mathbf{k}(T) \cdot \mathrm{grad}(T)] = G(r, z, T) \tag{7}$$

where $\mathbf{k}$ is a thermal conductivity tensor, T is temperature and G is a rate of heat generation per unit volume. Equation (7) is solved using the finite-element method assum-

ing the adiabatic boundary condition at the laser axis (imposed by the cylindrical symmetry of the modelled structure) and the first-type boundary condition (constant temperature) at the bottom surface of the laser heat sink. Boundary conditions based on the Newton equation and the Stefan–Boltzmann law are assumed to consider convective and radiative heat transfer from side and top walls of the laser chip. However, results of our calculations for the GaAs-based SDL show that these processes have a very limited influence on temperature within the laser volume, so they may be neglected in thermal simulations and the adiabatic boundary condition on side and top walls may be assumed as well [8]. Solving the heat transfer equation with the aid of the finite-element method is a typical approach to calculating temperature distribution within volumes of semiconductor lasers. However, there are different methods of determining heat sources in the laser active region. For example, in the model described in [5] heat sources are estimated only on the basis of pumping beam intensity profile. This method is quick and simple, but cannot be used in the case of laser over-threshold operation. The more complex method shown in paper [2] takes into account carrier recombination and thermalisation processes, however in this case a vertical diffusion of carriers is not considered. Our model of heat sources, described in the next paragraph, is strictly connected with the carrier transport model and enables more accurate calculations of heat flow in a SDL active region.

The heat generation rate G in Eq. (7) is determined for each element i of the (r, z) grid. First we assume normal incidence of the pumping beam, which means that the pumping beam travels along the z axis. For elements located outside the active region we can write the following formula using the Beer–Lambert–Bouguer law:

$$G_i = \frac{P_{\text{in},\,i}\{1 - \exp[-d_i \alpha_i(T)]\}}{d_i} f_p(r_i) \tag{8}$$

where $P_{\text{in},\,i}$ is power of pumping radiation entering the given element, d is the element thickness, α is absorption coefficient, f_p is a normalised radial distribution of pumping beam intensity and r_i is radial position of the element. For elements located in the active region, the heat generation rate is determined based on carrier recombination rates. For elements in barriers we use the following formula:

$$G_{b,\,i} = (A_i n_i + B_i n_i^2 + C_i n_i^3)(E_p - E_{b,\,i}) + (A_i n_i + C_i n_i^2) E_{b,\,i} + \sum_m S_{\text{afc},\,i}^{(m)} E_e^{(m)} \tag{9}$$

where A, B, C are monomolecular, bimolecular and Auger recombination coefficients, respectively, n is carrier density, E_p is energy of pumping photon, E_b is barrier energy bandgap, m is the index of the transverse mode, E_e is energy of emitted photon and $S_{\text{afc}} E_e$ is heat generation rate due to free-carrier absorption. The first component describes the thermalisation of carriers from energy E_p to E_b. The second component is

heat generation rate due to non-radiative recombinations: monomolecular and Auger one. For elements in the QWs, we use the following expression:

$$G_{\mathrm{QW},i} = (A_i n_i + B_i n_i^2 + C_i n_i^3)(E_p - E_l) + (A_i n_i + C_i n_i^3)E_l + \sum_m L_{\mathrm{st}}^{(m)}(E_p - E_e^{(m)}) \tag{10}$$

where E_l is the average energy of carrier transitions in the QW, $L_{\mathrm{st}}^{(m)}$ is the hole burning rate for the m-th transverse mode. The first component describes heat sources due to thermalisation of carriers which recombine spontaneously in the QW. The second component describes a heat generation rate due to non-radiative recombination and the third one – due to thermalisation of carriers which recombine in the stimulated way. Equations (9) and (10) show that the knowledge of the carrier distributions in the barriers and QWs is necessary for proper determination of heat sources in a laser active region. However, these distributions depend strongly on a temperature of this region. This means that carrier and temperature distributions have to be determined in the self -consistent regime using both modules for heat flow and carrier transport calculations.

4. Optical phenomena

To calculate reflectivity and longitudinal modes of SDL structures, we use the model based on the transfer matrix method (TMM). This approach has been described in our previous work [6]. To analyse propagation of transverse modes in an external cavity, we use the generalised *ABCD* law [9] for Gauss–Laguerre modes in stable optical resonators. All these modes are described by the complex beam parameter q

$$\frac{1}{q(z)} = \frac{1}{R(z)} - \frac{i\lambda_0\sqrt{2p+l+1}}{\pi n_R w_{pl}(z)}\sqrt{1+\left(\frac{z}{z_0}\right)^2} \tag{11}$$

where R is the radius of curvature of the phase front, w_{pl} is the beam radius defined via the second intensity moments for the Gauss–Laguerre mode described by p, l order numbers [9], λ_0 is beam's vacuum wavelength, n_R is the refractive index and z_0 is the Rayleigh range of the Gaussian beam. Propagation of the individual modes from a plane 1 to plane 2 through *ABCD*-type optics can be calculated using the *ABCD* law

$$q_2 = \frac{Aq_1 + B}{Cq_1 + D} \tag{12}$$

where q_1 is the initial beam parameter and q_2 is the resulting beam parameter after the beam has traversed the optical system described by the *ABCD* ray transfer matrix. It should be noted that q is the same for all Gauss–Laguerre modes. Therefore, we can determine the size w_{pl} for all modes by finding the q value only for the one chosen

mode, for example for the fundamental one. To find the complex beam parameter of a stable optical resonator, one needs to know the ray matrix of the cavity. Assuming a starting point, we find the *ABCD* matrix that goes through the cavity and return until the beam is in the same position and direction as the starting point. Since the beam parameter of resonator modes reproduces itself after each round trip, we make $q_0 = q_e$, where q_0 is the beam parameter for the starting point and q_e is the beam parameter after the round trip. Hence, using Eq. (12), we get the following equation:

$$Cq_e^2 + (D - A)q_e - B = 0 \tag{13}$$

Solving Eq. (13) gives the beam parameter for the chosen starting point. Then, using the Eq. (12), we can find the beam parameter for any other location in the laser cavity.

5. Self-consistent model

All model parts (for diffusion, thermal, optical and gain calculations) can be used as separated blocks to simulate individual physical phenomena, but also as a steady-state self-consistent model which takes into account a nonlinear interrelation between these processes. This model enables a complex analysis of SDL operation including determination of its output power characteristics. First, initial values of: material parameters, pumping power and output power for transverse modes are set. Then, calculations of heat flow, carrier transport, material gain and light propagation are carried out in the self-consistent regime. When a convergence for all modules is achieved, the program checks if carriers and power gains and losses are correctly balanced. If not, new values of the output power for the individual modes are set and next iteration of the calculation loop starts. New values of output power are determined using the following recurrence relation:

$$P_{i+1}^{(m)} = 2\pi \int \sum_k \left[L_{\mathrm{st}}^{(m,k)}(P_i^{(m)}, r) E_e^{(m)}(r) d_{\mathrm{QW}}^{(k)} \right] r \mathrm{d}r \tag{14}$$

where $P^{(m)}$ is output power for the m-th mode, i is iteration of the loop, k is the index of the QW, E_e is energy of the emitted photon, d_{QW} is the QW thickness. Calculations are carried out until the $P_{j+1}^{(m)} = P_j^{(m)}$ condition is met for each considered transverse mode (which corresponds to the condition that carrier and power gains and losses are correctly balanced). To the best of our knowledge, such a recurrence formula enabling self-consistent calculations for each transverse mode in SDL has not been presented so far. Applying this procedure to successive values of pumping power we can determine the whole power transfer characteristic of the modelled laser.

6. Carrier and power losses analysis

In this section we present results of a numerical analysis of carrier and power losses in the 1.3-μm GaInNAs/GaAs SDL carried out with the aid of the above described

self-consistent model. The modelled laser is based on the structure described in [10]. Its active region consists of five pairs of GaInNAs QWs separated by GaAs barriers. The DBR mirror is composed of 25.5 pairs of AlAs and GaAs quarter-wavelength layers. Over the active region there is the 282-nm-thick AlGaAs window layer for carrier confinement and the 10-nm-thick GaAs cap layer protecting bottom layers from oxidation. The epitaxial structure was grown on the 450-μm-thick GaAs substrate. The 270-μm-thick diamond layer of high thermal conductivity is bonded to the laser upper surface with the aid of capillary action to improve heat extraction efficiency. The laser structure is mounted on a copper water-cooled heat sink with the aid of an indium foil. The complete laser chip looks like the one shown in Fig. 1. The external optical cavity consists of the laser chip, high-reflectivity curved mirror and 2% output coupler (OC) and is set in a V-shape scheme. The laser is pumped by a diode array emitting at 810 nm. The pumping beam is focused down to 75-μm width on the laser upper surface with a three-lens arrangement.

Figure 3 presents a comparison between experimental results from [10] and results of calculations for the modelled laser. Figure 3**a** shows reflectivity and photoluminescence spectra of the epitaxial structure at 20°C. Figure 3**b** shows power transfer char-

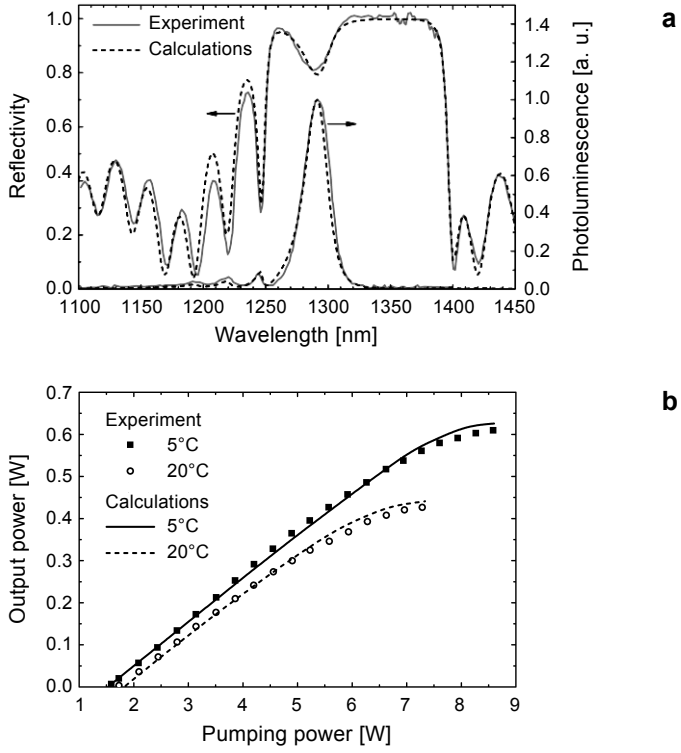

Fig. 3. Theoretical and experimental results for the 1.3-μm GaInNAs/GaAs SDL based on the structure from [10]: reflectivity and photoluminescence spectra of the epitaxial structure (**a**), output power *vs*. pumping power at 5°C and 20°C (**b**).

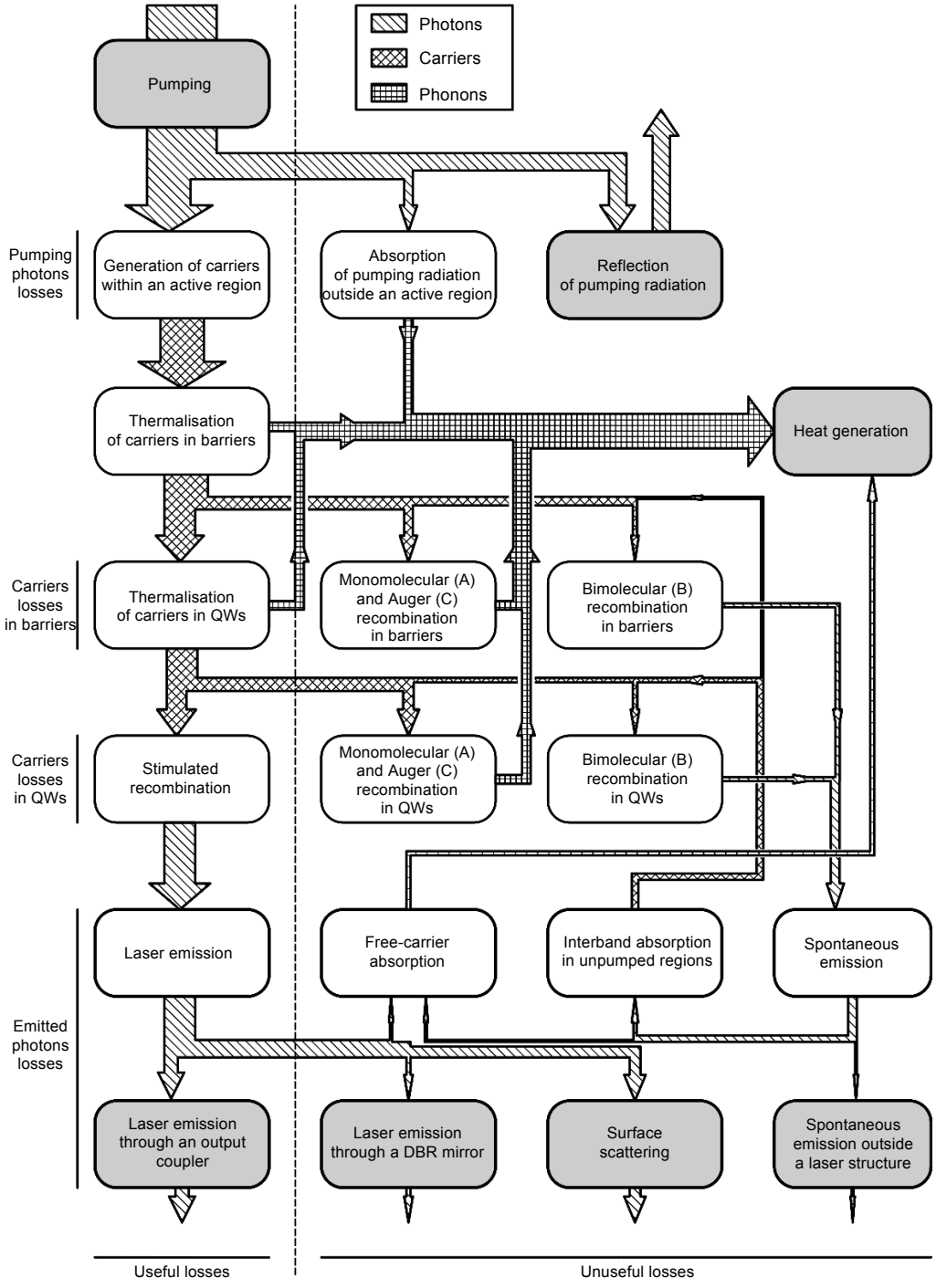

Fig. 4. Diagram of carrier and photon losses taken into consideration in the self-consistent SDL model.

acteristics (output power *vs*. pumping power) for two temperatures of the laser heat sink. In our calculations we have assumed 1.3% and 1.8% scattering coefficients at the air-diamond and diamond-semiconductor interfaces, respectively. A non-ideal thermal contact between the heat spreader and the epitaxial structure has been taken into account by inserting an additional 10-nm-thick layer of 0.42 W/(m·K) thermal conductivity between these two components. A good agreement between the experimental and theoretical results proves an accuracy of the presented model.

Figure 4 presents a diagram of carrier and power losses in SDL provided for in the described self-consistent model. Boxes contain names of physical phenomena taken into consideration in our simulations. The type of principal energy carriers – photons, charge carriers (called just carriers here) or phonons – participating in individual processes are denoted by arrows. The thickness of these arrows represents quantities of energy carriers estimated on the basis of our calculations for the GaInNAs/GaAs SDL. Therefore, although the diagram shows general principles underlying the SDL operation, the arrow thickness may vary depending on the structure geometry and material system, growth quality, pumping parameters and so on.

Individual power and carrier losses are discussed starting from the top of the diagram. First, we have pumping photon losses. Some part of pumping radiation is reflected from the laser surface (~21.5% in the modelled laser) and some part is absorbed in layers outside the active region (~13.5%). In the modelled structure only 65% of pumping radiation is absorbed in the active region. It means that the laser efficiency cannot exceed 65% in this case. A quantitative analysis of power and carrier losses in the laser active region of the modelled GaInNAs/GaAs SDL for pumping power 8.5 W and heat sink temperature 5°C is presented in Fig. 5. The diagram on the left shows a distribution of power of pumping radiation absorbed in the laser active region. The diagram on the right shows a distribution of carriers generated in the active region. About 8.8% of absorbed power is lost due to carrier thermalisation in barriers. The energy difference between energy of pumping photon and energy bandgap of barriers is converted into heat. Some of the carriers generated in barriers (1.5%) recombine

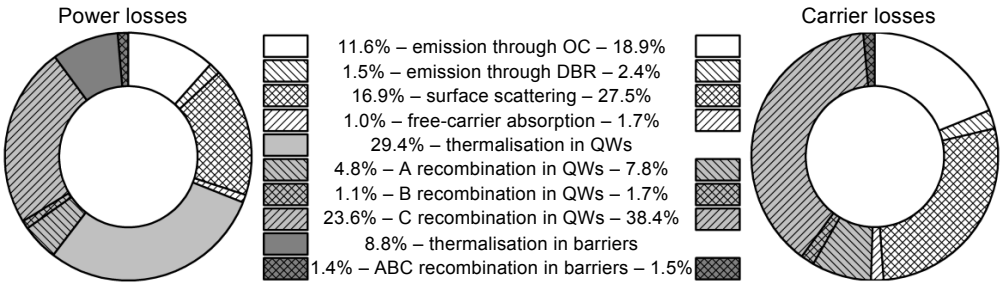

Fig. 5. Distribution of power of pumping radiation absorbed in the active region (power losses) and carriers generated in the active region (carrier losses). Results obtained for the 1.3 μm GaInNAs/GaAs SDL based on the structure from [10] for pumping power 8.5 W at 5°C. A, B and C – monomolecular, bimolecular and Auger recombinations, respectively.

through monomolecular, bimolecular (spontaneous radiative emission) and Auger recombination processes. Rest of them thermalise to energy levels in QWs. The excess energy is converted into heat. Carrier thermalisation in QWs is one of the strongest mechanisms limiting efficiency of SDLs. In the modelled laser 29.4% of absorber power is lost due to this process. Carriers in QWs may recombine through monomolecular (7.8%), bimolecular (1.7%) and Auger (38.4%) recombinations. Generally Auger recombination in QWs is a strong limit for high performance of SDLs. In the modelled laser 23.6% of absorbed power is lost due to this process. Rest of the carriers in QWs (~50% of all carriers generated in the modelled active region) recombine through a stimulated emission (above a lasing threshold). In the considered laser, the total power of emitted radiation is about 30% of power of pumping radiation absorbed in the active region. Emitted photons may escape the semiconductor structure through a DBR mirror, scatter on surface defects or be absorbed by free carriers. Rest of them escape the optical cavity through the output coupler and form the laser output beam. In the modelled SDL 18.9% of all carriers generated in the active region contribute to this emission. Power of laser radiation emitted trough the OC is 11.6% of power of pumping radiation absorbed in the active region and ~7.5% of power pumping radiation incident on the laser surface.

7. Conclusions

We have presented the numerical model of an optically pumped semiconductor disk laser. It consists of four main components for: carrier transport, heat flow, material gain and optical phenomena calculations. These components can be used as separate blocks to simulate individual physical processes or as the steady-state self-consistent model, which enables a complex analysis of both single- and multi-mode operation of semiconductor disk laser. Capabilities of this model have been presented by performing the analysis of power and carrier losses in the GaAs-based structure. The main mechanisms limiting SDL efficiency have been pointed out. This shows that the presented model may be a useful tool for designing and optimising new laser structures and predicting their future performance.

Acknowledgments – This work was partially supported by the National Science Centre, Poland (DEC-2014/15/N/ST7/05290, DEC-2012/07/D/ST7/02581 and DEC-2014/13/B/ST7/00633).

References

[1] KUZNETSOV M., *Semiconductor Disk Lasers: Physics and Technology*, [Ed.] Okhotnikov O.G., Wiley -VCH Verlag, 2010, pp. 1–71.

[2] ZAKHARIAN A.R., HADER J., MOLONEY J.V., KOCH S.W., BRICK P., LUTGEN S., *Experimental and theoretical analysis of optically pumped semiconductor disk lasers*, Applied Physics Letters **83**(7), 2003, pp. 1313–1315.

[3] GESKE J., GAN K.-G., OKUNO Y.L., PIPREK J., BOWERS J.E., *Vertical-cavity surface-emitting laser active regions for enhanced performance with optical pumping*, IEEE Journal of Quantum Electronics **40**(9), 2004, pp. 1155–1162.

[4] MOROZOV Y.A., LEINONEN T., HARKONEN A., PESSA M., *Simultaneous dual-wavelength emission from vertical external-cavity surface-emitting laser: a numerical modeling*, IEEE Journal of Quantum Electronics **42**(10), 2006, pp. 1055–1061.

[5] KEMP A.J., HOPKINS J.-M., MACLEAN A.J., SCHULZ N., RATTUNDE M., WAGNER J., BURNS D., *Thermal management in 2.3-μm semiconductor disk lasers: a finite element analysis*, IEEE Journal of Quantum Electronics **44**(2), 2008, pp. 125–135.

[6] SOKÓŁ A.K., SARZAŁA R.P., *Influence of pumping beam width on VECSEL output power*, International Journal of Electronics and Telecommunications **60**(3), 2014, pp. 239–245.

[7] SARZAŁA R.P., NAKWASKI W., *Optimization of 1.3 μm GaAs-based oxide-confined (GaIn)(NAs) vertical-cavity surface-emitting lasers for low-threshold room-temperature operation*, Journal of Physics: Condensed Matter **16**(31), 2004, article S3121.

[8] SOKÓŁ A.K., SARZAŁA R.P., *Thermal management of GaInNAs/GaAs VECSELs*, Opto-Electronics Review **21**(2), 2013, pp. 191–198.

[9] HODGSON N., HORST W., *Laser Resonators and Beam Propagation. Fundamentals, Advanced Concepts, Applications*, Springer, 2005.

[10] HOPKINS J.-M., SMITH S.A., JEON C.W., SUN H.D., BURNS D., CALVEZ S., DAWSON M.D., JOUHTI T., PESSA M., *0.6 W CW GaInNAs vertical external-cavity surface emitting laser operating at 1.32 μm*, Electronics Letters **40**(1), 2004, pp. 30–31.

Received November 7, 2015
in revised form January 21, 2016